

Weak Gravitational Lensing by a Sample of X-Ray Luminous Clusters of Galaxies – II. Comparison with Virial Masses¹

Ragnvald J. Irgens² and Per B. Lilje

*Institute of Theoretical Astrophysics, University of Oslo, P. O. Box 1029 Blindern,
N-0315 Oslo, Norway*

`per.lilje@astro.uio.no`

Håkon Dahle^{3,5}

NORDITA, Blegdamsvej 17, DK-2100 Copenhagen Ø, Denmark

and

S. J. Maddox⁴

School of Physics and Astronomy, University of Nottingham, Nottingham NG7 2RD, UK

ABSTRACT

Dynamic velocity dispersion and mass estimates are given for a sample of five X-ray luminous rich clusters of galaxies at intermediate redshifts ($z \sim 0.3$) drawn from a sample of 39 clusters for which we have obtained gravitational lens mass estimates. The velocity dispersions are determined from between 9 and 20 redshifts measured with the LDSS spectrograph of the William Herschel Telescope, and virial radii are determined from imaging using the UH8K mosaic CCD camera on the University of Hawaii 2.24m telescope.

Including clusters with velocity dispersions taken from the literature, we have velocity dispersion estimates for 12 clusters in our gravitational lensing sample. For this sample we compare the dynamical velocity dispersion estimates with our estimates of the velocity dispersions made from gravitational lensing by fitting a

²Present address: Telenor Broadband Services, P. O. Box 6914 St. Olavs plass, N-0130 Oslo, Norway

³Also at: Institute for Astronomy, University of Hawaii

⁴Also at: Institute of Astronomy, University of Cambridge

⁵Visiting observer, University of Hawaii 2.24m Telescope at Mauna Kea Observatory, Institute for Astronomy, University of Hawaii

singular isothermal sphere profile to the observed tangential weak lensing distortion as a function of radius. In all but two clusters, we find a good agreement between the velocity dispersion estimates based on spectroscopy and on weak lensing.

Subject headings: cosmology: observations — dark matter — galaxies: clusters: individual (Abell 914, Abell 959, Abell 1351, Abell 1576, Abell 1722, Abell 1995) — gravitational lensing — X-rays: galaxies: clusters

1. Introduction

Rich clusters of galaxies are probably the largest well-defined and gravitationally bound objects in the universe, and knowledge of their properties is not only interesting in itself, but can also set important constraints on models of large-scale structure formation. In particular, the cluster mass function has caught major interest (e.g., Bahcall & Cen 1993; Gross et al. 1998). Reliable estimates of cluster masses are also important in order to constrain the ratio of baryonic to total mass and to determine the density parameter Ω_0 (e.g., White & Frenk 1991; Lilje 1992; White, Efstathiou, & Frenk 1993; Carlberg et al. 1996; Eke, Cole, & Frenk 1996).

Cluster masses have been measured using different methods, having different biases and systematics. The method of cluster mass measurement with the longest history is the application of the virial theorem to positions and velocities of cluster galaxies. The first estimates of cluster masses were obtained by Zwicky (1933) and Smith (1936). They found that the total mass of galaxies in a cluster only accounted for a small portion of the total cluster mass. This method works well for low redshift clusters, where it can be based on a large number of galaxies, but has recently been applied also to galaxies at intermediate redshifts (e.g., Carlberg et al. 1996) where the number of galaxies observed per cluster is usually relatively small.

Other methods for mass measurement are based on analysis of gravitational lensing by the cluster and consequent distortion of background galaxies and measurements of the X-ray

¹Based on observations made with the William Herschel Telescope, operated on the island of La Palma by the Isaac Newton Group in the Spanish Observatorio del Roque de los Muchachos of the Instituto de Astrofísica de Canarias, and with the Nordic Optical Telescope, operated on the island of La Palma jointly by Denmark, Finland, Iceland, Norway, and Sweden, in the Spanish Observatorio del Roque de los Muchachos of the Instituto de Astrofísica de Canarias.

temperature of the hot intra-cluster medium. Of these, weak gravitational lensing has recently become frequently used for estimating the masses of clusters at intermediate and high redshifts (see e.g., recent reviews by Mellier [1999] and Bartelmann & Schneider [2001]). To understand systematic differences between the different mass estimators, comparative studies are necessary. Dahle et al. (2002; hereafter Paper I) presents weak lensing measurements of 39 highly X-ray luminous galaxies at redshift $0.15 < z < 0.35$ where the masses and their distributions have been determined homogeneously by up-to-date methods. In this paper we present velocity dispersion and virial mass estimates of five clusters from the sample of Paper I, which are compared with the weak lensing results. Our mass determinations are based on the method pioneered by Limber & Mathews (1960) where the mass estimator is

$$M_V = \frac{3\pi}{2} \frac{\sigma_P^2 R_H}{G}. \quad (1)$$

Here σ_P is the one-dimensional velocity dispersion of the cluster, while R_H is the projected mean harmonic point-wise separation (projected virial radius) defined by

$$R_H = \frac{N(N-1)}{\sum_{i < j} R_{ij}^{-1}}, \quad (2)$$

where N is the number of galaxies in the cluster and R_{ij} is the projected distance between any pair of galaxies. In our analysis we have used this method with the modifications of Carlberg et al. (1996) which are described later in the paper. To be able to use equation (1) or versions of it for estimating masses, one has to both determine the velocity dispersion of a cluster through spectroscopy and the angular distribution of cluster galaxies from photometric imaging.

In §2 we present our cluster sample and describe our observing and data reduction procedures for the spectroscopic and photometric observations of the sample. In §3 we determine the velocity dispersions of the clusters, while we in §4 use the photometric data to estimate the virial radii of the clusters. The virial mass estimates are presented in §5. Finally, in §6, we add to our sample a sample of seven clusters for which we have obtained weak lensing data and for which there exists velocity dispersions in the literature. The velocity dispersions of the clusters of this larger sample are compared with our weak lensing results.

2. Sample and Observations

Our clusters are taken from the weak lensing analysis sample of Paper I, and the selection criteria are described in detail there. That sample consists of 39 highly X-ray luminous

clusters in the redshift range $0.15 < z < 0.35$, taken from the samples of Briel & Henry (1993) and Ebeling et al. (1996, 1998). The six clusters selected for optical spectroscopic analysis, Abell 914, Abell 959, Abell 1351, Abell 1576, Abell 1722, and Abell 1995, were all in the Briel & Henry (1993) sample. Except from Abell 914, they were selected to have X-ray luminosities higher than 7×10^{44} erg s $^{-1}$ in the 0.5–2.5 keV ROSAT cluster rest frame band. With the revised redshift presented in this paper, also Abell 959 has a somewhat lower X-ray luminosity. The cluster redshifts (Huchra et al. 1990) are in the range 0.29–0.33, except for Abell 914 which is at $z = 0.19$. The data for Abell 959 were of poor quality because of clouds, and therefore that cluster is omitted from most of our analysis.

Our spectroscopic observations were made on the three nights, 1995 April 30 to May 3, with the LDSS-2 Low Dispersion Survey Spectrograph (Allington-Smith et al. 1994) at the 4.2m William Herschel Telescope (WHT) on La Palma. The LDSS-2 was used in a conventional multi-slit mode with slit width 1''.5 and with the medium grism. The slit length was typically 15''– 20'', which left adequate space for sky line subtraction around each galaxy (the half light radii of the galaxies were in the range 1''– 1''.5). We used one mask per cluster, with typically 30 to 40 slits in the 11' field. The detector was the thinned 1024² pixel Tektronix CCD TEK-1 with an angular scale of 0''.59 pixel $^{-1}$ giving a dispersion of 5.3Å pixel $^{-1}$. The FWHM seeing was typically 1''.1 – 1''.2 during the observations. The spectra normally covered the range 3500 to 8400Å, for some spectra the range was smaller.

Target galaxies were chosen based on magnitude and morphology (color information was not used) from images taken at the Nordic Optical Telescope (also at La Palma), coordinates were determined from the APM Sky Catalogue⁶, and the slit positions of the different masks were then determined in the standard way. Each cluster mask was observed with three exposures, each of 1.8 ks duration, giving a 5.4 ks combined exposure of each field. Dispersed flat-fields of the twilight sky and of a tungsten lamp were taken for each mask. Before each cluster observation, an exposure was made of a CuAr wavelength calibration lamp with high signal-to-noise lines in the range 5400Å–7500Å. Flux calibration exposures were made of a number of spectrophotometric standard stars.

The data were reduced by the LEXT package (Colless et al. 1990; Allington-Smith et al. 1994). The data reduction included bias subtraction, correction for distortion effects, flat-fielding, combination of exposures, sky subtraction, extraction of one-dimensional spectra, and wavelength- and flux calibration. The data reduction procedure took into account flexure differences between exposures and geometric distortions in the LDSS-2 optics. The optimal extraction routine of Horne (1986) was utilized. The wavelength calibration was based on

⁶<http://www.ast.cam.ac.uk/~mike/apmcat/>

third-order polynomial fits to the CuAr arc lines, and in general provided rms residuals less than 0.2\AA for wavelengths between 5400\AA and 8000\AA , which is the range used to determine the redshifts. A typical reduced one-dimensional spectrum of an early-type galaxy in one of our clusters is shown in Figure 1.

The individual one-dimensional spectra were analyzed with the utility **crcor** which was kindly provided by Dr. W. J. Sutherland. Its main estimation method is the cross correlation technique of Tonry & Davis (1979), but all spectra are also searched for emission lines. In our case, the cross correlation was done with a set of 18 template spectra, using galaxy spectra from Kennicutt (1992) and stellar spectra from Jacoby, Hunter, & Cristian (1984). The cross correlation routine gives an estimate of the redshift, the significance of the redshift and its mean error, and it also assigns a quality flag ranging from 0 to 4. If emission lines are found, a quality flag for the emission line redshift is also assigned based on the number of identified lines and their strength. All spectra were also checked manually. The cross correlation method was preferred if it gave a quality flag equal to or better than the emission line quality flag. In general, redshifts with quality flag 3 or better were found to be trustworthy, and were used in the analysis. Spectra with quality flag ≤ 2 were discarded, unless they were confirmed by manual inspection. The data for Abell 959, which were collected during partial cloud cover, only yielded five good galaxy redshifts. For the other clusters, the number of good spectra range from 13 (Abell 1722) to 24 (Abell 1995). The estimated redshift error was typically $50\text{--}100\text{ km s}^{-1}$. One of the objects in Abell 1995 was not a galaxy, but a quasar at $z = 2.66$. Its coordinates (J2000.0) are $\alpha = 14^{\text{h}}53^{\text{m}}08.9^{\text{s}}$ and $\delta = 58^{\circ}03'11.9''$. It is located about $90''$ east of the central galaxy of Abell 1995, and a simple singular isothermal sphere gravitational lens model with a velocity dispersion 1200 km s^{-1} (which is consistent with our weak gravitational lensing data) implies that the QSO is magnified by a factor 1.5 by the cluster potential.

To determine the angular distribution of cluster galaxies, photometric imaging of the cluster fields were performed at the University of Hawaii 2.24m telescope (UH2.2m) at Mauna Kea, Hawaii during three observing runs, 1998 February 19–23, 1999, May 14–16, and 2000 March 8–11, using the $8\text{k} \times 8\text{k}$ pixel UH8K mosaic CCD camera in the f/10 Cassegrain focus. Further details of these observations and the reduction procedures of the data are given in Paper I. The UH8K instrument has eight $4\text{k} \times 2\text{k}$ CCDs and has a field of view of $19'$ by $19'$, enough to fit not only the central parts, but also most of the outer regions of the clusters. However, chip # 4 located in the NE corner was not used in our analysis, as it had poor cosmetic quality. The data were run through a data processing pipeline consisting of pre-processing of the original images, transformation from chip to celestial coordinates and warping and averaging to produce the final images. These final UH8K images were rebinned into $2\text{k} \times 2\text{k}$, giving $0''.6\text{ pixel}^{-1}$ resolution for the analysis reported in this paper.

3. Cluster redshifts and velocity dispersions

In our case, the number of observed galaxies per cluster was modest, ranging from 13 to 24 (and for Abell 959 where it was not possible to determine a velocity dispersion, five). It is obvious that estimates of the cluster redshifts and especially velocity dispersions (and the mass estimator is proportional to the square of the velocity dispersion, see eq. [1]) must rely on utilizing the most robust estimators with high resistance to avoid problems caused by e.g., deviations from Gaussian velocity distribution and contamination from foreground and background galaxies. In our analysis, we used the optimal estimators for contaminated galaxy samples of this size (Beers, Flynn, & Gebhardt 1990), the biweight estimators of location and scale, as estimators for the cluster redshifts and velocity dispersions, respectively. Confidence intervals were calculated using the bias corrected and accelerated bootstrap method (Efron 1987) with 10,000 bootstrap replications. These robust estimators and methods for determining confidence intervals have been well tested on redshift samples like ours (except from Abell 959, see e.g., Beers et al. 1990; Girardi et al. 1993; Borgani et al. 1999). For the biweight estimator of location, we chose a value for the tuning constant ($c = 6.0$) that gave the estimator good robustness and high efficiency. For example, in the case of a sample approximating a Gaussian distribution, the rejection point is $cMAD \equiv 4$ standard deviations from the median, where MAD ($= 0.6745$ in the Gaussian case) is the median absolute deviation from the sample median (for details, see e.g., Mosteller & Tukey 1977). For the biweight estimator of scale, we chose a tuning constant $c = 9.0$ such that in the Gaussian case, galaxies more than 6 standard deviations away from the median would be rejected. Our statistical analysis was performed using the ROSTAT program kindly provided by Dr. T. C. Beers. A single iteration was performed for the biweight measurements.

Our redshift and velocity dispersion estimates are presented in Table 1. The analysis uses only galaxies with well measured redshifts which have not been rejected as foreground or background objects. The second column in Table 1, N , shows the number of galaxy redshifts used in each cluster. The third and fourth columns show the derived cluster redshift and the derived one-dimensional velocity dispersion together with 68% confidence limits. Given the modest number of spectroscopically measured galaxies in each cluster, we performed an additional estimate of the errors associated with small-number statistics to check if they were compatible with the confidence intervals in Table 1. This was done by repeatedly drawing random samples of galaxies (with $N = 10$ and $N = 20$) from a much larger redshift data set ($N \simeq 200$; see Yee et al. 1996) for Abell 2390 ($z = 0.23$), which has a velocity dispersion of $\sigma_P = 1093 \pm 61 \text{ km s}^{-1}$ (Carlberg et al. 1996). The variance in the values for the redshift and velocity dispersion calculated from 100 such subsamples is similar to, or slightly ($< 30\%$) larger than, the confidence intervals in Table 1.

Table 1. Cluster redshifts and velocity dispersions

	N	z	σ_P (km s^{-1})	z (H90) ^a	N (H90) ^b
Abell 914	11	$0.1934^{+0.0017}_{-0.0012}$	1140^{+290}_{-170}	0.1941	3
Abell 959	4 ^c	$0.2857^{+0.0034}_{-0.0034}$...	0.3530	2
Abell 1351	17	$0.3279^{+0.0014}_{-0.0015}$	1680^{+340}_{-230}	0.3220	3
Abell 1576	14	$0.2986^{+0.0011}_{-0.0013}$	1040^{+170}_{-120}	0.3020	1
Abell 1722	9	$0.3264^{+0.0013}_{-0.0017}$	970^{+280}_{-130}	0.3275	1
Abell 1995	20	$0.3207^{+0.0010}_{-0.0010}$	1130^{+150}_{-110}	0.3180	2

^aLiterature redshift (Huchra et al. 1990).

^bNumber of individual galaxy redshifts measured by Huchra et al. (1990).

^cWith only four cluster galaxies with measured redshifts in the Abell 959 field, a velocity dispersion could not be estimated. The confidence interval for the cluster redshift was estimated from the variance in the results obtained by randomly drawing redshift values from a much larger data set for a similar cluster (see the text for details).

For most of our six clusters, the determined redshifts are in relatively good agreement with previous results (Huchra et al. 1990), but ours are based on a much larger number of galaxy redshifts. However, for Abell 959 where we only base our cluster redshift on four galaxies, our redshift is significantly lower than the redshift of Huchra et al. (1990). Three of the four galaxies that we based our redshift estimate on have $V - I$ colors putting them in the middle of the red sequence of the color-magnitude diagram of the field. Both the galaxies used by Huchra et al. (1990) were substantially bluer than the cluster red sequence. We therefore believe that our cluster redshift for Abell 959 is correct. The 68% confidence limits for the redshift of this cluster could not be reliably estimated using the bootstrap method we used for the other clusters, and the confidence limits shown in Table 1 are instead based on the variance in the results obtained by drawing 4 galaxies at random from the Yee et al. (1996) data set for Abell 2390.

Struble & Rood (1999) list a redshift of $z = 0.279$ for Abell 1576, significantly lower than the value we derive from our data and the value measured by Huchra et al. (1990). The lower redshift value (which is also the one given by NED) originates from a study by Leir & van den Bergh (1977) and is an estimate based on a combination of cluster galaxy photometry and cluster richness. We note that Abell 1351, where the measurement is based on 17 redshifts, has an abnormally high velocity dispersion. This is partially confirmed by the weak lensing analysis (see §6). Patel et al. (2000) have recently published redshift and velocity dispersion measurements of Abell 1995, based on the redshifts of 15 galaxies, six of which are common with our data set. Their result of $z = 0.322 \pm 0.001$ and $\sigma_P = 1282^{+153}_{-120} \text{ km s}^{-1}$ agrees quite well with our result.

4. Angular distribution of cluster galaxies

As described in §1, the virial mass estimator (eq. 1) traditionally uses the projected mean harmonic point-wise separation defined in equation (2). However, this estimator is sensitive to close pairs and is somewhat noisy (see e.g., Carlberg et al. 1996). It will also systematically underestimate the radius for a rectangular aperture when the entire cluster is not covered (Bahcall & Tremaine 1996). Carlberg et al. (1996) proposed to instead use a related radius, the ring-wise projected harmonic mean radius, defined by

$$\begin{aligned} R_h &= \frac{N(N-1)}{\sum_{i < j} \frac{1}{2\pi} \int_0^{2\pi} \frac{d\theta}{\sqrt{R_i^2 + R_j^2 + 2R_i R_j \cos \theta}}} \\ &= \frac{N(N-1)}{\sum_{i < j} \frac{2}{\pi(R_i + R_j)} K(k_{ij})}, \end{aligned} \tag{3}$$

where R_i and R_j are the distances of galaxies i and j from the cluster center, $k_{ij}^2 = 4R_iR_j/(R_i+R_j)^2$ and $K(k)$ is the complete elliptic integral of the first kind in Legendre’s notation. This radius treats one of the particles in the pairwise potential $|\mathbf{R}_i - \mathbf{R}_j|^{-1}$ as having its mass distributed like a ring around some given cluster center and is less noisy and handles non-circular apertures better than the standard R_H . It will, however, overestimate the true projected virial radius if the cluster is significantly flattened or extensive sub-clustering is present. In our analysis we therefore use both methods to check the influence of the choice of radius in the virial mass estimator on the uncertainty of the resulting virial mass.

The radii R_h and R_H should in principle be computed for all galaxies residing in the virialized regions of each cluster. In our case, we have only measured redshifts of a few galaxies in each field, and redshifts can therefore not be used to select likely cluster galaxies over which these sums are to be taken. Instead we use the UH8K photometry described in §2 to select the cluster galaxies. Our procedures for object detection and classification follow Kaiser, Squires, & Broadhurst (1995), and are described in detail in Paper I. Briefly, we first ran a peak finding algorithm with a 4σ detection limit. Then we performed aperture photometry on the detected objects and removed stellar objects brighter than $I = 21^m$ by applying cuts in the size-magnitude diagram. After having removed stars and very faint objects (the completeness limit is $I \sim 25.0^m$), the V - and I -catalogs were combined. In the final catalog we kept objects that were detected in both V and I with positions that differed by less than $1''.2$ (2 pixels). The peak finding algorithm of Kaiser et al. (1995) is optimised for detecting small, faint galaxies, and may occasionally have problems resolving closely grouped galaxies in cluster cores. To test whether our choice of galaxy detection algorithm had a significant influence on our results, we also calculated R_H values from galaxy catalogs generated using the SExtractor object finding algorithm (Bertin & Arnouts 1996). The resulting variations in the R_H values were small and within the quoted uncertainty intervals. In addition, the performance of the Kaiser et al. (1995) detection algorithm was tested by examining images of the cluster fields with the catalog object positions superposed on the galaxies.

In a color-magnitude diagram (see Fig. 2 for Abell 1351), the cluster galaxy red sequence consisting of early type galaxies is clearly visible (see also e.g., Olsen [2000]). We exploited this fact in our procedures for discriminating cluster members from galaxies possibly belonging to background or foreground structures. As described in detail in Paper I, we generated catalogs of “cluster” galaxies by making appropriate cuts in each cluster color-magnitude diagram to include early type galaxies at the cluster redshift. We also tried to use galaxy samples that included all galaxies in the fields down to a certain magnitude limit without any color selection. This did not produce significant changes in the results, except for Abell 1351, which displays clear evidence of a foreground structure (the color-magnitude diagram for this

cluster clearly shows an additional red sequence at $V - I \sim 1.2$). To assess the uncertainty in the analysis caused by some arbitrariness in the exact positions of the color cuts, we varied the limits of the cuts to make an ensemble of galaxy catalogs for each cluster on which the further analysis was performed in parallel. To determine R_h , the position of the cluster center is needed. This was found in two steps, first by applying a peak finding algorithm on a smoothed map of the distribution of galaxies defined to be cluster members by the color criteria described above. As described later in this chapter, we chose three different sets of galaxies within three different radii from this center to perform our analysis. For each of these sets we recomputed the center which we used for determining R_h . The center was set to be the biweight estimate (Beers et al. 1990) of the mean of the x and y coordinates of all galaxies used in the estimate. We tested for the effect of varying the center position, and found that varying this by less than 50 pixels did not significantly affect the results.

The radius entering the virial mass estimator (eq. 1), and hence the mass estimate itself, can be biased if we include galaxies outside the virialized part of the cluster, or vice versa, if we exclude galaxies outside some radius within the virialized part of the cluster. The projected density distribution of galaxies outside the cluster core is well known to fall approximately $\propto R^{-1}$ both in the virialized region and in the surrounding infalling region (reflected in the cluster-galaxy cross-correlation function [e.g., Lilje & Efstathiou 1988]). Thus we would not expect to see a visible border between the virialized region and the infalling region. This is confirmed by our data. However, it is normally assumed (see e.g., Carlberg et al. 1996) that the virialized region encompasses the region around the cluster center where the average density is about 200 times the critical density of the universe. This is based on the fact that in the Einstein de Sitter universe, a purely spherical top-hat perturbation will virialize at a density 178 times the background density at the time of virialization. In other universe models, the value is somewhat different, and in open models all clusters virialize at an epoch much earlier than the present epoch. However, the figure 200 is sufficient as an approximate estimate (see e.g., Lilje 1992). For a typical rich cluster this is the region within a radius quite close to the Abell radius ($1.5h^{-1}\text{Mpc}$). Our $19'$ by $19'$ field is about two Abell radii across at the typical cluster redshifts, so our field is approximately of the right size to minimize this possible bias. In our analysis, we compute R_H and R_h both using all “cluster” galaxies in the field, and for only the galaxies within radii of 6 respectively 8 arcminutes from the cluster center. The scatter between these three different estimates of the radii estimated from the same cluster was normally of the order of 10%. There was a systematic effect, in that the estimated radii to some extent scaled with the size of the cutoff. We use the differences in these results to determine the uncertainty in our final virial mass determinations. As seen in Figure 3 where the positions of all “cluster galaxies” in a typical catalog for Abell 1351 are shown as circles, most of the galaxies defined as “cluster”

galaxies in each field do indeed reside within the inner of these radii. Before doing our analysis we also had to mask certain areas in the fields and reject galaxies in those areas from our analysis. Those areas included the UH8K CCD # 4 and the areas surrounding bright stars. For Abell 914, the cluster was not positioned in the center of the field but in the NW quadrant, to be able to simultaneously image another cluster in the SE quadrant. For Abell 914 we therefore only used galaxies in the NW $15' \times 15'$ part of the mosaic in our analysis.

For each cluster we constructed three ensembles of “cluster” galaxy catalogs, using the whole image, the central $8'$ field and the central $6'$ field. Each ensemble consisted of about 5 catalogs where the color and magnitude selection criteria for “cluster” galaxies had been varied within reasonable bounds. For each catalog in all these ensembles we computed R_H (eq. 2) and R_h (eq. 3). For all the ensembles, R_h differed from R_H by less than 5%, and we chose to only use R_h in our further analysis. We express R_h in length units assuming an Einstein de Sitter cosmology ($\Omega_0 = 1, \Lambda = 0$). If we instead had assumed a cosmology with $\Omega_0 = 0.3$ and $\Lambda = 0.7$, the radii would have become 13% larger at $z = 0.3$ and 9% larger at $z = 0.2$. Compared to our other uncertainties, this error is relatively small. Finally, we express the radius used in our further virial mass analysis as the deprojected virial radius,

$$r_V = \frac{\pi}{2} R_h. \quad (4)$$

Dr. T. C. Beers’ ROSTAT program (described in §3) was then applied to the combined ensemble of estimates of r_V for each cluster to find the best estimate of its r_V (by the biweight estimator of location), and the 68% confidence limits on this estimate (by the bias corrected and accelerated bootstrap method). With the systematic effect mentioned above, i.e., a correlation between the estimated R_h and the radius within which galaxies have been picked for analysis, it is clear that this method has its deficiencies. It does not necessarily give an unbiased estimate of the expectancy value of r_V , and the estimated confidence limits cannot be treated as formal 68% confidence limits. However, with the rather large uncertainties in these estimates, the quoted confidence limits give a fair estimate of the uncertainty in the results, which are of order 10%. Our results are presented in the second column of Table 2. Since the small number of redshifts for Abell 959 prevented us from finding its velocity dispersion, we also omitted it from the galaxy distribution analysis.

5. Cluster virial masses

The virial masses of the clusters, given by equation (1), are shown in the third column of Table 2. The given statistical errors are based on half the length of the 68% confidence

intervals of the cluster velocity dispersions and virial radii, and standard propagation of errors.

The virial mass given by equation (1) and Table 2 is the mass of the virialized region of the cluster, supposed to be within the virial radius r_V . Since the density profile in the outer parts of the virialized region, and at least the inner part of the infalling region, in a cluster is close to being $\propto r^{-\alpha}$ where $2 \lesssim \alpha \lesssim 3$ (e.g., Adami et al. 1998; Carlberg et al. 1996; Lilje & Efstathiou 1988), this mass can be scaled to other radii assuming that the mass inside a given radius grows approximately proportional to the radius.

As pointed out in §4, there is no clear feature seen in clusters at the transition from the virialized region to the surrounding infalling region. Also, the idea of a virialized region bounded in space by a spherical border, surrounded by the non-virialized infalling region, is clearly an oversimplification. There might well be recently infallen galaxies or subclusters within the virial radius which have not been virialized, and these will bias the mass estimate. Also, we know that real clusters may be far from spherical. Even the quite large statistical errors given in Table 2, should therefore be taken with a pinch of salt, because of the uncertainty in what the derived virialized mass really measures.

Even for our idealized model, there are also several other possible sources for systematic errors. If our measurement only uses galaxies inside a bounding radius r_b much smaller than the virial radius, our mass estimate will be an overestimate of the mass within r_b because of the neglect of the surface term in the virial theorem (Carlberg et al. 1996). This effect is at most 50%. Our virial radius estimates of §4 were derived assuming an Einstein-de Sitter cosmology. As pointed out in that chapter, this overestimates the virial radius, and hence the virial mass, by about 10% if the real universe is vacuum energy dominated with $\Omega_0 \sim 0.3$.

6. Comparison with weak lensing measurements

In Paper I we derived weak lensing mass estimates for a sample of 39 galaxy clusters including the clusters studied in this paper. Seven additional clusters from the Paper I sample have spectroscopically determined velocity dispersion measurements available in the literature. Here, we compare these measurements to the velocity dispersion estimates σ_{WL} derived in Paper I by fitting a singular isothermal sphere (SIS) profile to the observed tangential weak lensing distortion as a function of radius. We note, however, that three of the clusters (Abell 959, Abell 1351 and Abell 1576) were poorly fit by a SIS profile.

In Table 3 we summarize the available data for the clusters discussed in this paper, and the available data for the clusters with published velocity dispersion measurements for which

we have weak lensing data.

The quantity σ_{DM} ($= \sigma_{\text{WL}}$ listed in Paper I) in the fourth column of Table 3 is derived from the weak lensing results of Paper I. A subsample of 11 clusters have spectroscopically measured velocity dispersions σ_P , which are plotted against the dark matter velocity dispersions σ_{DM} in Figure 4.

There is generally a reasonably good agreement between σ_P and σ_{DM} , with a tendency for the former to be smaller than the latter by a barely significant amount, the median value of $\sigma_P/\sigma_{\text{DM}}$ being 0.94. We also find $\langle \sigma_P/\sigma_{\text{DM}} \rangle = 1.02 \pm 0.13$ when using all twelve clusters and $\langle \sigma_P/\sigma_{\text{DM}} \rangle = 0.97 \pm 0.08$ after excluding two outliers mentioned below. If we only consider the clusters for which we have measured σ_P in this paper (but excluding Abell 914, for reasons given below), we find $\langle \sigma_P/\sigma_{\text{DM}} \rangle = 0.98 \pm 0.12$.

One cluster (Abell 914, at $z = 0.194$) shows a σ_P a factor ~ 2 larger than σ_{DM} , with a very strong ($> 2\sigma$) discrepancy between the two velocity dispersion values. However, there is a second cluster (Abell 922, at $z = 0.189$) at a projected distance of only 11 arcminutes on the sky. Since the weak lensing measurements indicate that Abell 922 is a more massive cluster than Abell 914 (its estimated σ_{DM} is $810_{-130}^{+120} \text{ km s}^{-1}$), the observed redshifts, which were measured in a $10' \times 10'$ field centered on Abell 914, may have been significantly contaminated by galaxies along the line of sight belonging to the other cluster.

A second cluster (Abell 697, at $z = 0.282$) shows an almost equally strong discrepancy in the opposite direction, with $\sigma_{\text{DM}} \sim 2 \times \sigma_P$. We note however, that the spectroscopically measured galaxy velocity dispersion is based on a rather small number of cluster galaxies ($N = 9$; see Metzger & Ma 2000).

7. Discussion

Our in general good agreement between σ_P determined from dynamical estimates and σ_{DM} determined from gravitational lensing estimates contrast other results.

Smail et al. (1997) presented a comparison of weak lensing and spectroscopic mass measurements for a sample of 9 clusters at $0.17 < z < 0.55$ which were imaged with the WFPC2 instrument aboard the Hubble Space Telescope (HST). They compared the average tangential shear observed within an annulus around the optical cluster center ($60 < r < 200h^{-1} \text{ kpc}$) to the expected shear from SIS-type mass profile with the observed galaxy velocity dispersion. The shear signal was found to be significantly lower than predicted from the spectroscopic measurements for all the clusters, and Smail et al. (1997) suggested that

this was caused by systematic overestimates (by typically $\sim 50\%$) of the cluster velocity dispersion values given in their paper. As noted in §6, we see no such discrepancy in our data. Hoekstra et al. (2001) argue that this discrepancy is instead a result of the small field size of the single WFPC2 pointings used by Smail et al. (1997) to measure the gravitational shear. If there is significant substructure in the central regions of the clusters, or if the density profiles of the clusters are significantly shallower than a SIS-type model at small radii, the shear measurements are likely to underestimate the true cluster mass.

Brainerd et al. (1999) have used ray-tracing through high-resolution N -body simulations of massive ($M_V \sim 10^{15} h^{-1} M_\odot$) clusters to show that the average tangential shear, when measured within an annulus with an outer radius R_{MAX} significantly smaller than the virial radius (and assuming a SIS-type mass profile), will tend to underestimate the true cluster mass. For $R_{\text{MAX}} \simeq R_V$, they find that the SIS-model fit yields quite accurate mass values (typically 5% – 10% underestimates; see their Figure 9) even if the true mass density profile of the clusters is more accurately represented by the model proposed by Navarro, Frenk, & White (1995). We note that for most of the clusters listed in Table 3, we have estimated σ_{DM} based on tangential shear measurements out to radii $\simeq R_V$ (for most of our clusters, we have used $R_{\text{MAX}} = 550'' = 1.5 h^{-1} \text{Mpc}$ at $z = 0.3$; see Paper I for details), so we expect our values to be essentially unbiased.

Girardi & Mezzetti (2001) have reanalyzed the available radial velocity measurements in the clusters studied by Smail et al. (1997) and derive velocity dispersion values that are on average about 20% lower than those given by Smail et al. (1997). Thus, it appears that the discrepancy between spectroscopic and lensing mass estimates seen by Smail et al. (1997) is most probably caused by a simultaneous overestimation of dynamical masses and underestimation of lensing masses, of almost equal magnitude. Girardi & Mezzetti (2001) also compare their virial cluster mass estimates with weak lensing mass estimates drawn from the literature for 18 clusters (for 7 of these the lensing mass was measured from single HST WFPC2 pointings), and find a median value $M_{\text{spec}}/M_{\text{lens}} = 1.30$ and a 90% confidence interval $0.63 < M_{\text{spec}}/M_{\text{lens}} < 2.13$. This is consistent with our results in §6 within the errors, but the M_{lens} values they use are probably subject to a larger bias caused by the (on average) significantly smaller fields used to measured the shear.

In their study, Brainerd et al. (1999) did not consider the possible effect of structures outside their clusters on the lensing mass estimates. Galaxy clusters are believed to be connected by large filaments of dark matter, diffuse gas, and galaxies, and mass within such filaments will contribute significantly to the lensing mass when seen in projection along the line of sight to a cluster, even if it is physically separated from the cluster by several Mpc (Metzler, White, & Loken 2001). Still, even in this scenario, σ_{DM} may not necessarily be

significantly larger than σ_P , since the galaxy velocity dispersion would also be biased upwards by galaxies outside the virial radius falling into the main cluster along the filaments.

The modest fraction ($\sim 30\%$) of massive clusters that have significant substructure in their dark matter distribution provide evidence that the majority of massive clusters at $z = 0.2\text{--}0.3$ are close to dynamical equilibrium (Dahle et al. 2002a). The good agreement that we find between virial masses and lensing masses for most of our clusters is consistent with this picture, although significant amounts of substructure could probably be present in the clusters without changing the σ_P values beyond the error bounds of our measurements. To reliably assess the dynamical state of the clusters from spectroscopic data alone, it would probably be necessary to observe galaxy samples an order of magnitude larger than those we present in this paper. In addition, X-ray observations, particularly using Chandra and XMM, would be an efficient aid to measure substructure and determine the dynamical state of the clusters. We plan to investigate the relation between weak lensing and X-ray properties for a larger sample of clusters in a future paper (H. Dahle et al. 2002b, in preparation).

We thank Dr. T. C. Beers for letting us use his ROSTAT statistical analysis program and Dr. W. J. Sutherland for providing us his redshift measurement utility `crcor`. We thank the staff of the William Herschel Telescope, the University of Hawaii 2.2m Telescope and the Nordic Optical Telescope for support during our observing runs. HD gratefully acknowledges the Research Council of Norway for a doctoral research fellowship. RJI, PBL and HD thank the Research Council of Norway for travel support. This research has made use of the NASA/IPAC Extragalactic Database (NED) which is operated by the Jet Propulsion Laboratory, California Institute of Technology, under contract with the National Aeronautics and Space Administration.

Table 2. Cluster Virial Radii and Masses

	r_V (h^{-1} Mpc)	M_V ($10^{15}h^{-1}M_\odot$)
Abell 914	$1.23^{+0.13}_{-0.12}$	1.1 ± 0.6
Abell 1351	$1.68^{+0.18}_{-0.13}$	3.3 ± 1.4
Abell 1576	$1.52^{+0.10}_{-0.21}$	4.0 ± 1.4
Abell 1722	$1.86^{+0.22}_{-0.19}$	1.2 ± 0.6
Abell 1995	$1.19^{+0.15}_{-0.20}$	1.1 ± 0.4

Note. — The values are given for an Einstein-de Sitter Universe. See the text for a brief discussion of possible additional systematic uncertainties that are not included in the error intervals given here.

Table 3. Cluster data.

Designation	z	σ_P	Ref.	σ_{DM}	L_{X} (0.1–2.4 keV)
		(km s $^{-1}$)	σ_P	(km s $^{-1}$)	10^{44} erg s $^{-1}$
Abell 115	0.197	1074^{+208}_{-121}	(1)	1130^{+210}_{-270}	14.59 ^a
Abell 520	0.203	988 ± 76	(2)	1050 ± 100	14.52 ^b
Abell 665	0.182	821^{+233}_{-130}	(1)	1010^{+150}_{-170}	15.69 ^b
Abell 697	0.282	941 ± 296	(3)	1730^{+190}_{-200}	19.15 ^b
Abell 914	0.193	1141^{+153}_{-120}	...	540^{+160}_{-190}	5.00 ^b
Abell 959 ^c	0.286	990^{+100}_{-110}	14.3 ^b
Abell 963	0.206	1350^{+200}_{-150}	(4)	1070^{+150}_{-160}	8.72 ^b
Abell 1351	0.328	1680^{+340}_{-229}	...	1410^{+80}_{-90}	8.31 ^b
Abell 1576	0.299	1041^{+153}_{-183}	...	1060 ± 90	11.52 ^b
Abell 1722	0.326	966^{+283}_{-132}	...	1160 ± 140	9.70 ^b
Abell 1995 ^d	0.321	1126^{+151}_{-105}	...	1240 ± 80	13.42 ^b
Abell 2104	0.153	1200 ± 200	(5)	1390 ± 180	7.89 ^e
Zwicky 7160	0.258	1133 ± 140	(2)	1230 ± 130	13.73 ^b

References. — (1) Girardi & Mezzetti 2001, (2) Carlberg et al. 1996, (3) Metzger & Ma 2000, (4) Lavery & Henry 1998, (5) Liang et al. 2000

^aX-ray luminosity measured by Ebeling et al. (1998).

^bX-ray luminosity measured by Böhringer et al. (2000).

^cThe values have been corrected for the revised redshift for Abell 959 presented in this paper.

^dPatel et al. (2000) measure $\sigma_P = 1282^{+153}_{-120}$ for Abell 1995.

^eX-ray luminosity measured by Ebeling et al. (1996).

REFERENCES

Adami, C., Mazure, A., Katgert, P., & Biviano, A. 1998, *A&A*, 336, 263

Allington-Smith, J., et al. 1994, *PASP*, 106, 983

Bahcall, J. N. & Tremaine, S. 1981, *ApJ*, 244, 805

Bahcall, N. A. & Cen, R. 1993, *ApJ*, 407, L49

Bartelmann, M. & Schneider, P. 2001, *Physics Reports*, 340, 291

Beers, T. C., Flynn, K., & Gebhardt, K. 1990, *AJ*, 100, 32

Böhringer, H. et al. 2000, *ApJS*, 129, 435

Borgani, S., Girardi, M., Carlberg, R. G., Yee, H. K. C., & Ellingson, E. 1999, *ApJ*, 527, 572

Brainerd, T. G., Wright, C. O., Goldberg, D. M., & Villumsen, J. V. 1999, *ApJ*, 524, 9

Briel, U. G. & Henry, J. P. 1993, *A&A*, 278, 379

Carlberg, R. G., Yee, H. K. C., Ellingson, E., Abraham, R., Gravel, P., Morris, S., & Pritchett, C. J. 1996, *ApJ*, 462, 32

Colless, M., Ellis, R. S., Taylor, K., & Hook, R. N. 1990, *MNRAS*, 244, 408

Dahle, H., Kaiser, N., Irgens, R. J., Lilje, P. B., & Maddox, S. J. 2002, *ApJS*, 139, 313 (Paper I)

Ebeling, H., Voges, W., Böhringer, H., Edge, A.C., Huchra, J. P., & Briel, U.G. 1996, *MNRAS*, 281, 799

Ebeling, H., Edge, A. C., Böhringer, H., Allen, S., Crawford, C. S., Fabian, A.C., Voges, W., & Huchra, J. P. 1998, *MNRAS*, 301, 881

Efron, B. 1987, *Journal of the American Statistical Association*, 82, 171

Eke, V. R., Cole, S., & Frenk, C. S. 1996, *MNRAS*, 282, 263

Girardi, M., Biviano, A., Giuricin, G., Mardirossian, F., & Mezzetti, M. 1993, *ApJ*, 404, 38

Girardi, M & Mezzetti, M. 2001, *ApJ*, 548, 79

Gross, M. A. K., Somerville, R. S., Primack, J. R., Holtzman, J., & Klypin, A. 1998, MNRAS, 301, 81

Hoekstra, H., Franx, M., Kuijken, K., & van Dokkum, P. G. 2001, preprint (astro-ph/0109445)

Horne, K. 1986, PASP, 98, 609

Huchra, J. P., Henry, J. P., Postmann, M., & Geller, M. J. 1990, ApJ, 365, 66

Jacoby, G. H., Hunter, D. A., & Christian, C. A. 1984, ApJS, 56, 257

Kaiser, N., Squires, G., & Broadhurst, T. 1995, ApJ, 449, 460

Kennicutt, R. C. 1992, ApJS, 79, 255

Lavery, R. J. & Henry, J. P. 1998, BAAS, 30, 864

Leir, A. A. & van den Bergh, S. 1977, ApJS, 34, 381

Liang, H., Lémonon, L., Valtchanov, I., Pierre, M., & Soucail, G. 2000, A&A, 363, 440

Lilje, P. B. 1992, ApJ, 386, L33

Lilje, P. B. & Efstathiou, G. 1988, MNRAS, 231, 635

Limber, N. D. & Mathews, W. G. 1960, ApJ, 132, 286

Mellier, Y. 1999, ARA&A, 37, 127

Metzger, M. R. & Ma, C.-P. 2000, AJ, 120, 2883

Metzler, C. A., White, M., & Loken, C. 2001, ApJ, 547, 560

Mosteller, F. & Tukey, J. W. 1977, Addison-Wesley Series in Behavioral Science: Quantitative Methods, Reading, Mass.: Addison-Wesley, 1977

Navarro, J. F., Frenk, C. S., & White, S. D. M. 1995, MNRAS, 275, 720

Olsen, L. F. 2000, Ph.D. thesis, Copenhagen University

Patel, S. K. et al. 2000, ApJ, 541, 37

Smail, I., Ellis, R. S., Dressler, A., Couch, W. J., Oemler, A., Sharples, R. M., & Butcher, H. 1997, ApJ, 479, 70

Smith, S. 1936, *ApJ*, 83, 23

Struble, M. F. & Rood, H. J. 1999, *ApJS*, 125, 35

Tonry, J. & Davis, M. 1979, *AJ*, 84, 1511

White, S. D. M., Efstathiou, G., & Frenk, C. S. 1993, *MNRAS*, 262, 1023

White, S. D. M. & Frenk, C. S. 1991, *ApJ*, 379, 52

Yee, H. K. C., Ellingson, E., Abraham, R. G., Gravel, P., Carlberg, R. G., Smecker-Hane, T. A., Schade, D., & Rigler, M. 1996, *ApJS*, 102, 289

Zwicky, F. 1933, *Helv. Phys. Acta*, 6, 110

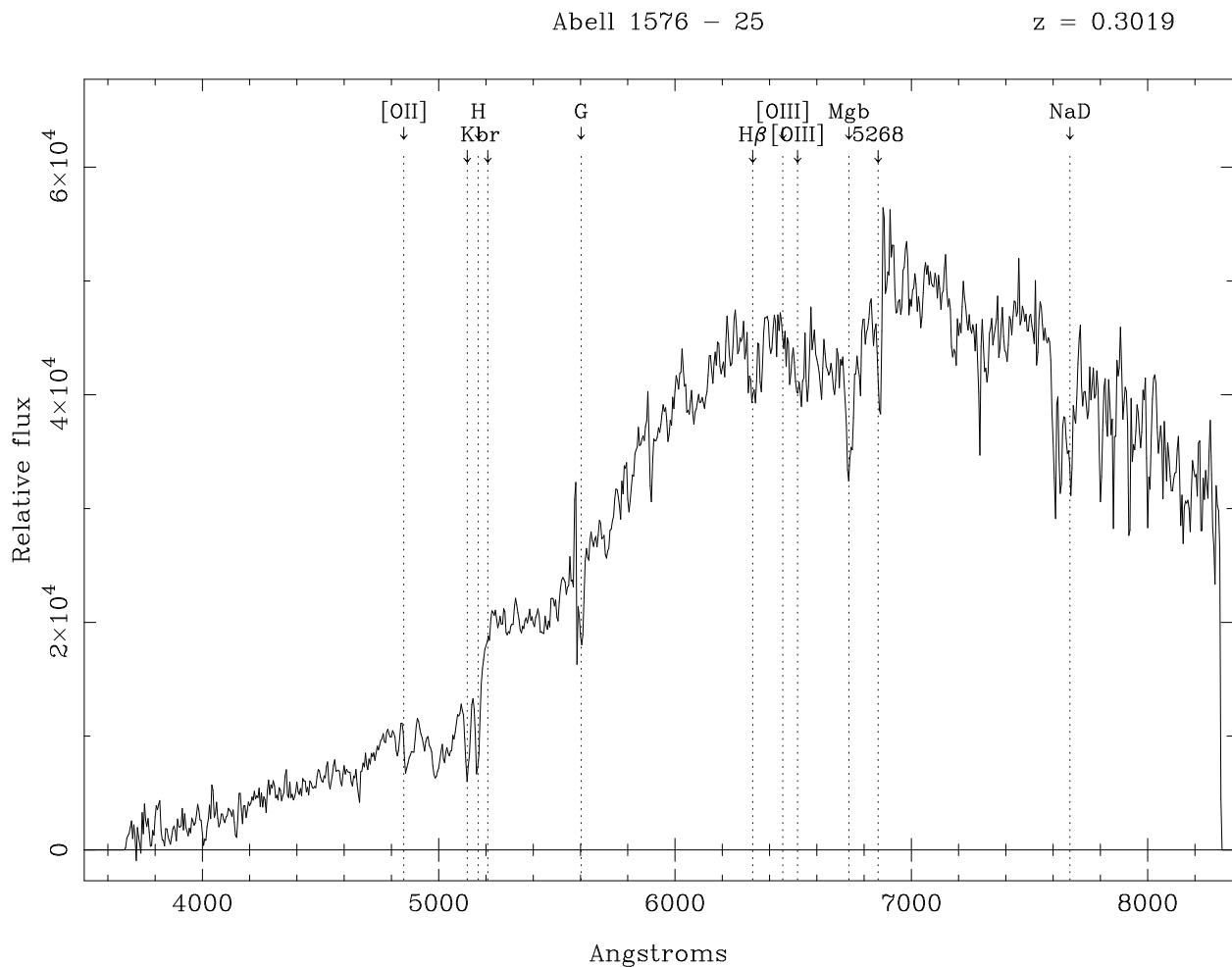


Fig. 1.— Spectrum of an early type galaxy in Abell 1576 with $z = 0.302$.

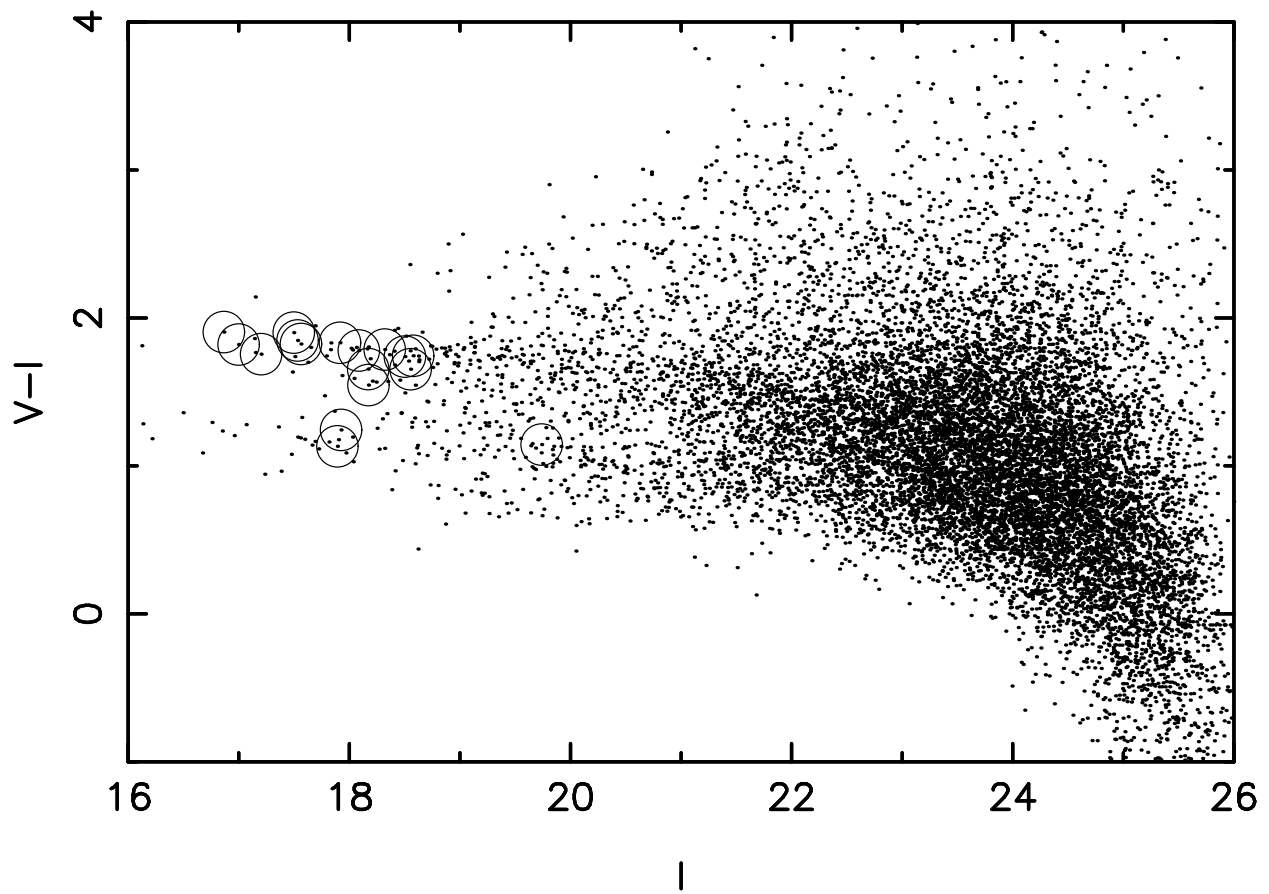


Fig. 2.— Color-magnitude diagram for Abell 1351. The positions of the galaxies with measured redshifts and colors are plotted with open circles. With a few exceptions, the selected galaxies are all within the main cluster sequence.

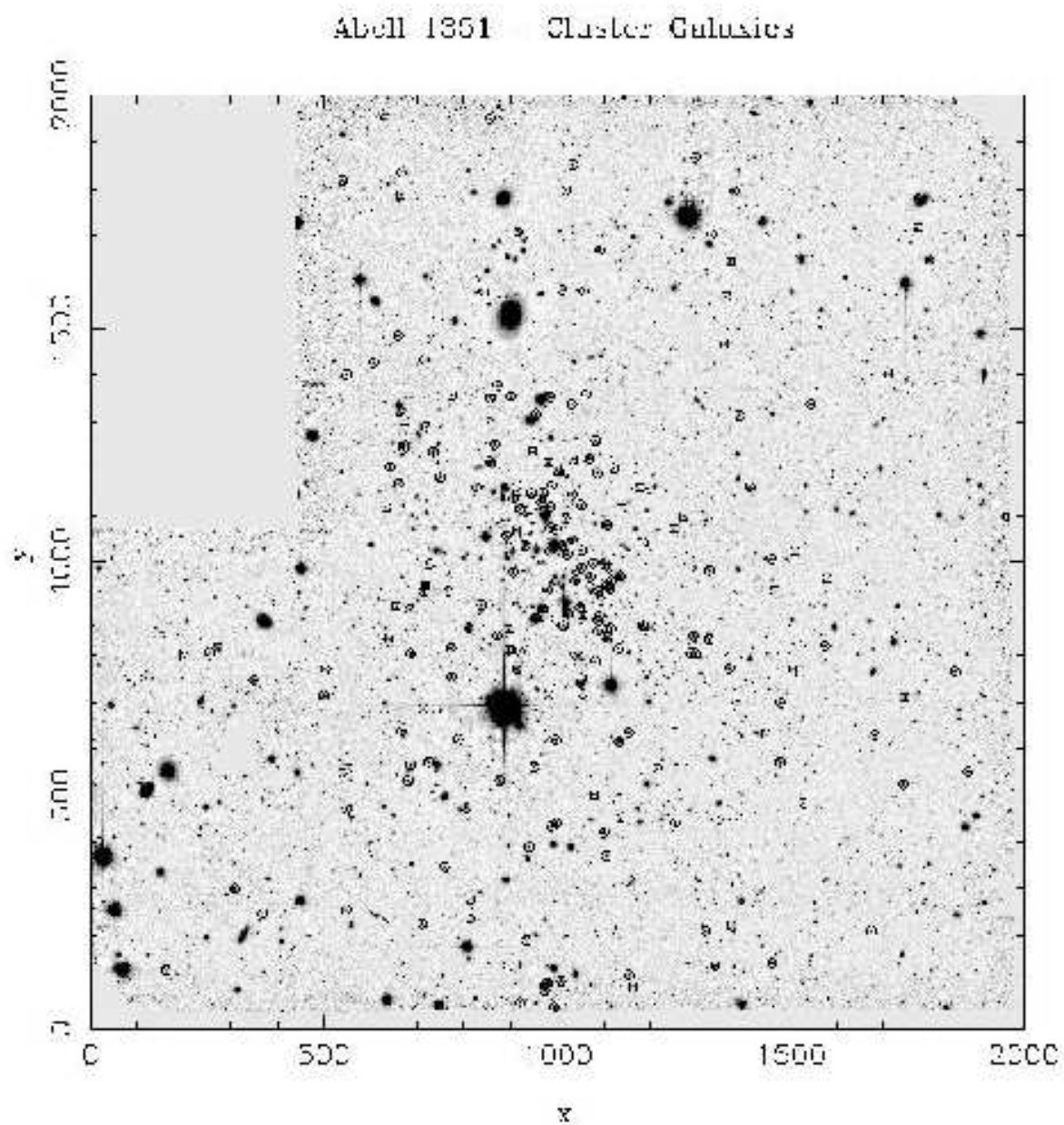


Fig. 3.— Image of Abell 1351 overlaid positions of cluster galaxies identified for the color-magnitude diagram (circles). In this figure, north is up, east is left and the scale on the axes is in pixels of size $0''.6$.

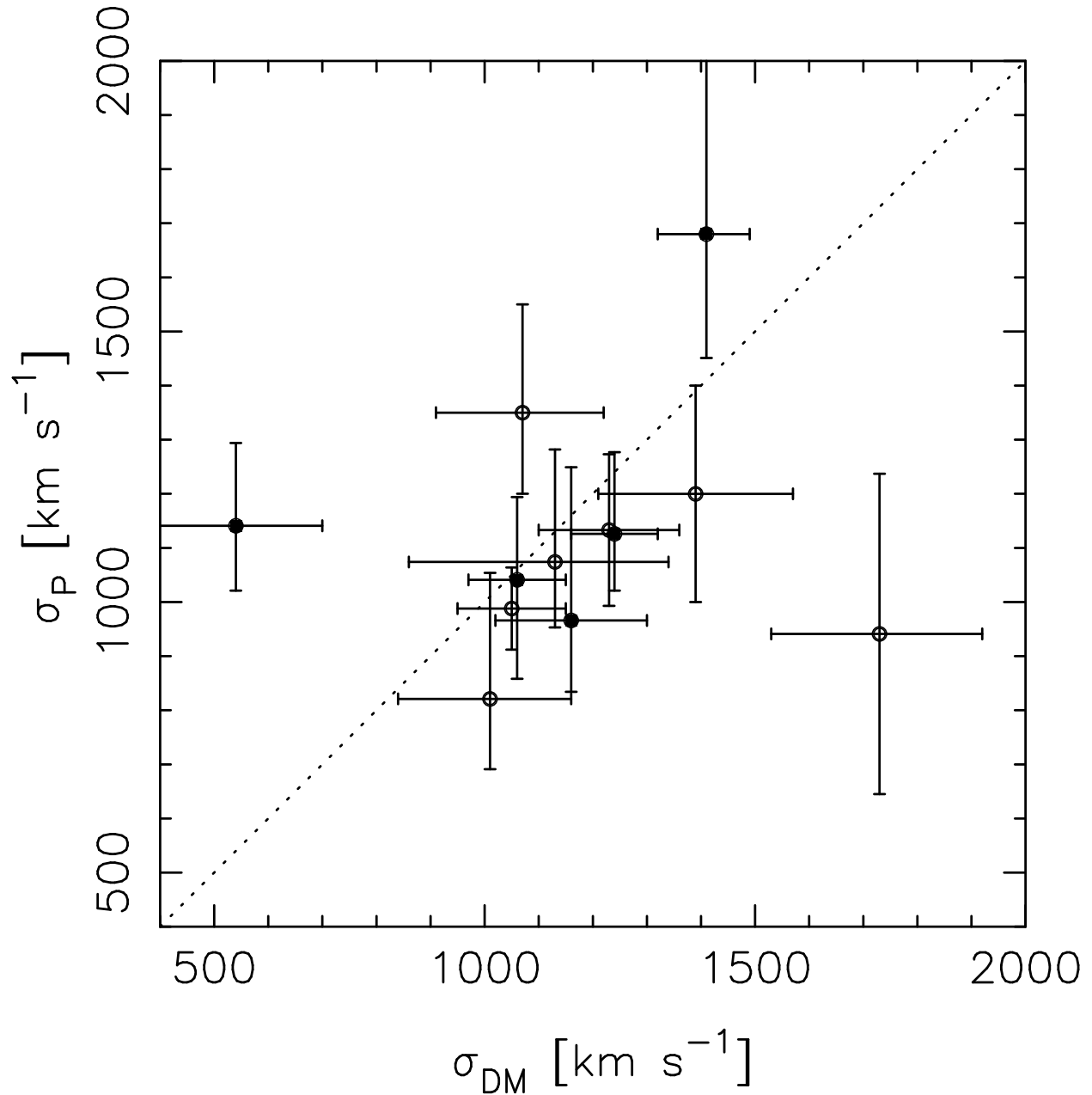


Fig. 4.— The spectroscopically measured velocity dispersion σ_P vs. the dark matter velocity dispersion σ_{DM} . The error bars shown are at 1σ . The dotted line indicates equality between the values. Filled circles represent the clusters for which we present σ_P measurements in this paper. The other points have σ_P values drawn from the literature.